

The union of rotational and vibrational modes in generator-coordinate-type calculations, with application to neutrinoless double-beta decay

Changfeng Jiao and Calvin W. Johnson

Department of Physics, San Diego State University, San Diego, California 92182-1233, USA

(Dated: September 30, 2019)

Good many-body methods for medium and heavy nuclei are important. Here we combine rotational motion with vibrational modes in a novel generator-coordinate method (GCM): starting from a mean-field solution (Hartree-Fock-Bogoliubov), we create non-orthogonal reference states from low-lying quasiparticle Tamm-Dancoff modes, and then project onto states of good angular momentum and particle number. The results we benchmark against full shell model calculations. Even with just a few such modes we find improvement over standard GCM calculations in excitation spectra. We also find significant improvement in $0\nu\beta\beta$ nuclear matrix elements.

For tests of fundamental symmetries such as neutrinoless double-beta ($0\nu\beta\beta$) decay [1–3], and investigations into astroparticle physics such as direct detection of dark matter [4–6], one needs accurate interaction matrix elements for medium- to heavy-mass nuclides. Despite a portfolio of available methods [7, 8] including recent developments [9–11], the nuclear many-body problem remains numerically challenging.

Among available methods, the configuration-interacting shell model (SM) is appealing for its intuitive interpretation, straightforward implementation, and wide usage both phenomenologically [12, 13] and *ab initio* [14, 15]. SM calculations boil down to diagonalizing in an orthonormal basis a second-quantized (occupation space) Hamiltonian [7],

$$\hat{H} = \sum_{ij} \epsilon_{ij} \hat{a}_i^\dagger \hat{a}_j + \frac{1}{4} \sum_{ijkl} V_{ijkl} \hat{a}_i^\dagger \hat{a}_j^\dagger \hat{a}_l \hat{a}_k, \quad (1)$$

where $\hat{a}_i^\dagger, \hat{a}_i$ are fermion creation and annihilation operators for single-particle states labeled by i, j, k, l . The downside of the SM method, however, is that in order to include relevant correlations, one needs a large number of basis states, and the dimension of the many-body basis increases exponentially with the number of valence nucleons and/or the number of single-particle states. This limits the numerically exact diagonalization of SM Hamiltonian to light nuclei or nuclear models with relatively few valence particles.

Alternatively, one can build correlations by diagonalizing the Hamiltonian in a small basis of nonorthogonal states. Here there are two branches. The first fall under the rubric of generator coordinate methods (GCM) [8, 16], while the second is known as the Monte Carlo shell model (MCSM)[17, 18]. In this paper we propose a novel approach to the GCM: we combine using angular momentum projection to extract rotational motion, with using low-lying vibrational modes to generate a set of reference states. Our initial results, applied to $0\nu\beta\beta$ transition matrix elements, show promising improvements over common GCM approaches.

The GCM is itself an application of the Hill-Wheeler equation [8], $\int \langle \Psi(\lambda') | \hat{H} | \Psi(\lambda) \rangle d\lambda = E \int \langle \Psi(\lambda') | \Psi(\lambda) \rangle d\lambda$,

where λ is some parameter which in practice is discretized. In GCM the (discretized) set of $\{|\Psi(\lambda)\rangle\}$, or reference states, are typically either particle-number conserving Slater determinants, or quasiparticle vacua, and are typically found by minimizing

$$\langle \Psi(\lambda) | \hat{H} - \lambda \hat{Q} | \Psi(\lambda) \rangle, \quad (2)$$

where λ is now a Lagrange multiplier, and \hat{Q} is some external field, the exact choice of which is part of the art of GCM; often there are several external fields and corresponding Lagrange multipliers. When using quasiparticles there are Lagrange multipliers, here suppressed, to constrain the number of protons and neutrons. Thus one solves constrained Hartree-Fock (HF) or constrained Hartree-Fock-Bogoliubov (HFB) equations for several different values of λ (and possibly different \hat{Q}) and traditionally one interprets either λ or, more commonly, the expectation value $\langle \Psi(\lambda) | \hat{Q} | \Psi(\lambda) \rangle$, as a generalized “coordinate” that “generates” the basis, hence the name. Of course, for $\lambda = 0$ one has the original HF or HFB equations. It is useful to imagine an energy landscape in the space of Slater determinants or quasiparticle vacua: the HF or HFB state is at the global minimum, and GCM explores the energy landscape around that minimum. Because these simple states almost always break rotational symmetry, and in the case of HFB, particle-number conservation, one needs to restore good angular momentum and particle number through projection. It is through the process of projection and then the mixing of multiple projected reference states, that one builds up important correlations. Angular momentum projection on deformed states in particular picks out rotational bands, and very often the excitation spectrum from a single angular-momentum projected state looks like a rotational band, even if the low-lying spectrum in the full space is not dominated by such bands.

An important question to answer is how to choose the external field(s) \hat{Q} and thus the non-orthogonal reference states. GCM calculation typically focus on collective correlations known to be important in nuclei. Most prominent are quadrupole deformations, originally with axial symmetry [19, 20] but later extended to triaxially-deformed configurations [21–24]. There are also stud-

ies in consideration of octupole modes [25, 26], as well as investigations of fluctuations in like-particle pairing [27, 28]. Recent work has indicated the transition operators of double-beta ($\beta\beta$) decay are sensitive to proton-neutron (pn) pairing correlations [29–32]. The inclusion of pn pairing correlations in GCM calculations [24, 33–35] significantly reduces the large difference in the $0\nu\beta\beta$ nuclear matrix elements between previous GCM and SM predictions [24, 34, 35]. Despite this success, even if one treats both quadrupole deformation and pn pairing as coordinates, and uses the same SM Hamiltonian, the $0\nu\beta\beta$ matrix elements of ^{124}Sn , ^{130}Te , and ^{136}Xe given by GCM are still overestimated by about 30% when compared with SM results [35]. This implies that some other correlations should not be neglected for an accurate description of $0\nu\beta\beta$ decay, and perhaps other nuclear properties. In addition, previous GCM work neglects, for the most part, non-collective correlations. How to pin down all the collective and non-collective correlations that may play relevant roles is still an open question.

Instead of choosing the constraining fields by hand, we let the system itself dictate the reference states, through the use of a theorem of Thouless [8]: the exponential of any one-body operator \hat{Z} acting on a Slater determinant $|\Psi\rangle$ is another Slater determinant $|\Psi'\rangle$,

$$\exp(\hat{Z})|\Psi\rangle = |\Psi'\rangle \equiv |\Psi(Z)\rangle. \quad (3)$$

Here we use Thouless’ theorem as applied to quasiparticle vacua to define an energy landscape $E(Z) = \langle\Psi(Z)|\hat{H}|\Psi(Z)\rangle$, which can be expanded in Z . Setting the first derivatives with respect to Z to be zero yields the Hartree-Fock/HFB equations. The second derivatives, which approximate the landscape as a quadratic in Z and thus a multi-dimensional harmonic oscillator, lead to the Tamm-Dancoff and random-phase approximations [8], and their quasiparticle extensions, for excited states. Closely related to this is the derivation of the random phase approximation from a generator coordinate picture [36].

(We note that the Monte Carlo shell model[17, 18], itself inspired by the imaginary-time-evolution auxiliary-field path-integral approach to the SM[37, 38], uses Thouless’ theorem to stochastically explore the energy landscape. One can relate the path integral, and thus the MCSM, to the random phase approximation [39]. While we do not sample the energy surface stochastically, the relationship between Thouless’ theorem, the energy landscape, the auxiliary-field path integral method, and the MCSM, inspired our development.)

Although one can work in a particle-conserving formalism (indeed, we are exploring this approach separately) for this paper we focus on quasiparticles. In this formalism, detailed below, excited states are modeled as collective linear combinations of two-quasiparticle excitations, with low-lying collective modes found by diagonalizing the Hamiltonian in this space, also known as the quasiparticle Tamm-Dancoff approximation (QTDA). Because they arise from a harmonic approximation to

the landscape, one can conceive of them as *vibrational* modes.

Here is where we branch from the default GCM. Rather than exploring the energy landscape by guessing (albeit with good reason) the important external fields, we solve the QTDA equations, identify the lowest QTDA (vibrational) modes, and use these modes to generate reference states via Thouless’ theorem. We then project out states of good angular momentum and particle number and diagonalize the Hamiltonian in this basis.

This is related to previous work which builds reference states using two-quasiparticle excitations [40, 41]. However those calculations simply used the lowest-lying two-quasiparticle excitations, whereas we use collective superpositions of two-quasiparticle excitations as given by QTDA. It is important to note that use of Thouless’ theorem is key to introducing general linear combinations of two-quasiparticle states.

In what follows we first briefly sketch the framework of QTDA-driven GCM, including the QTDA operators, Thouless evolution, symmetry restoration, and configuration mixing. We then use it to compute the low-lying level spectra, reduced $E2$ transition probabilities, and $0\nu\beta\beta$ decay matrix elements, compared with the results given by the SM and the GCM using quadrupole deformations and pn pairing amplitudes as coordinates (denoted as “CHFB-GCM”). Finally, we summarize our conclusions and suggest future work.

The founding HFB state $|\Phi_0\rangle$, found by minimizing (2) albeit only with constraints on proton and neutron numbers, is a vacuum to quasiparticles $\hat{c}_\alpha(0)$:

$$\hat{c}_\alpha(0) = \sum_{\beta} \hat{a}_{\beta} U_{\beta\alpha}^*(0) + \hat{a}_{\beta}^{\dagger} V_{\beta\alpha}^*(0), \quad (4)$$

where the argument ‘0’ indicates that $|\Phi_0\rangle$ is the vacuum relative to these quasiparticles, so that $\hat{c}_\alpha(0)|\Phi_0\rangle = 0$. This is important as our reference states will be a set of non-orthogonal vacua.

Low-lying excited states are approximated as linear combinations of two-quasiparticle excitations (the equivalent of particle-hole states in particle-conserving schemes with a Slater determinant): $\hat{Z}_r|\Phi_0\rangle$ where

$$\hat{Z}_r = \frac{1}{2} \sum_{\alpha\alpha'} Z_{\alpha\alpha'}^r \hat{c}_{\alpha}^{\dagger}(0) \hat{c}_{\alpha'}^{\dagger}(0). \quad (5)$$

To get the (antisymmetric) coefficients $Z_{\alpha\alpha'}^r$ of the QTDA operator, one computes the matrix elements of the Hamiltonian in a basis of two-quasiparticle excited states

$$A_{\alpha\alpha',\beta\beta'} = \langle\Phi_0|[\hat{c}_{\alpha'}(0)\hat{c}_{\alpha}(0), [\hat{H}, \hat{c}_{\beta}^{\dagger}(0)\hat{c}_{\beta'}^{\dagger}(0)]]|\Phi_0\rangle \quad (6)$$

The matrix \mathbf{A} is the quasiparticle Tamm-Dancoff (QTDA) matrix, and its expression in terms of the Hamiltonian matrix elements (1) and the quasiparticle transformation (4) is found in the literature [8, 42]. We solve

$$\sum_{\beta\beta'} A_{\alpha\alpha',\beta\beta'} Z_{\beta\beta'}^r = E_r^{\text{QTDA}} Z_{\alpha\alpha'}^r. \quad (7)$$

finding excitation energies E_r^{QTDA} . We approximate the QTDA states by applying Thouless' theorem:

$$\begin{aligned} |\Phi_r\rangle &= \exp(\lambda \hat{Z}_r) |\Phi_0\rangle \approx |\Phi_0\rangle + \lambda \hat{Z}_r |\Phi_0\rangle \\ &= \exp\left\{ \lambda \frac{1}{2} \sum_{\alpha\alpha'} Z_{\alpha\alpha'}^r \hat{c}_\alpha^\dagger(0) \hat{c}_{\alpha'}^\dagger(0) \right\} |\Phi_0\rangle. \end{aligned} \quad (8)$$

While in principle we could sample different values of λ similar to the integration over auxiliary fields in the path integral method, we found in our current work that a single value of $\lambda = 1$ worked sufficiently well.

With application of Thouless' theorem we have a new quasiparticle vacuum $|\Phi_r\rangle$, and we need to file new quasiparticle states $\hat{c}_\alpha(r)$ that annihilate it. Application of Thouless' theorem with particle-hole operators on a Slater determinant is straightforward[37], but much less so for quasiparticle vacua. We follow the development of [43], defining the intermediate operators

$$\tilde{c}_\alpha(r) = \hat{c}_\alpha(0) + \lambda \sum_{\mu} \hat{c}_\beta^\dagger(0) Z_{\beta\alpha}^r \quad (9)$$

which satisfy $\tilde{c}_\alpha(r) |\Phi_r\rangle = 0$. However, they are not proper quasiparticle operators, as they do not satisfy fermion anti-commutation relations:

$$\left\{ \tilde{c}_\alpha(r), \tilde{c}_{\alpha'}^\dagger(r) \right\} = \delta_{\alpha\alpha'} + \lambda^2 \sum_{\mu} Z_{\mu\alpha}^r Z_{\mu\alpha'}^{r*}, \quad (10)$$

We regain proper anti-commutation relations by defining

$$\mathbf{L}\mathbf{L}^\dagger = \mathbf{I} + \lambda^2 \mathbf{Z}^T \mathbf{Z}^*. \quad (11)$$

where \mathbf{I} is the unit matrix, and \mathbf{L} is a lower triangular matrix found easily by a Cholesky decomposition, which is inverted, and then defining

$$\hat{c}_\alpha(r) = \sum_{\alpha'} L_{\alpha\alpha'}^{-1} \tilde{c}_\alpha(r), \quad (12)$$

which have the desired anti-commutation relations,

$$\begin{aligned} \left\{ \hat{c}_\alpha(r), \hat{c}_{\alpha'}^\dagger(r) \right\} &= \sum_{\mu\mu'} L_{\alpha\mu}^{-1} [L_{\alpha'\mu'}^{-1}]^* \left\{ \tilde{c}_\mu(r), \tilde{c}_{\mu'}^\dagger(r) \right\} \\ &= \left(\mathbf{L}^{-1} (\mathbf{I} + \lambda^2 \mathbf{Z}^T \mathbf{Z}^*) [\mathbf{L}^{-1}]^\dagger \right)_{\alpha\alpha'} = \delta_{\alpha\alpha'}. \end{aligned} \quad (13)$$

The resultant Bogoliubov transformation matrix of the transformed state $|\Phi_r\rangle$ is given by $\begin{pmatrix} \hat{c}^\dagger(r) \\ \hat{c}(r) \end{pmatrix} =$

$$\begin{aligned} &\begin{pmatrix} [\mathbf{L}^{-1}]^* & \lambda [\mathbf{L}^{-1} \mathbf{Z}^T]^* \\ \lambda \mathbf{L}^{-1} \mathbf{Z}^T & \mathbf{L}^{-1} \end{pmatrix} \begin{pmatrix} \mathbf{U}(0)^T & \mathbf{V}(0)^T \\ \mathbf{V}(0)^\dagger & \mathbf{U}(0)^\dagger \end{pmatrix} \begin{pmatrix} \hat{a}^\dagger \\ \hat{a} \end{pmatrix} \\ &= \begin{pmatrix} \mathbf{U}(r)^T & \mathbf{V}(r)^T \\ \mathbf{V}(r)^\dagger & \mathbf{U}(r)^\dagger \end{pmatrix} \begin{pmatrix} \hat{a}^\dagger \\ \hat{a} \end{pmatrix} \end{aligned} \quad (14)$$

where

$$\begin{aligned} \mathbf{U}(r) &= (\mathbf{U}(0) + \lambda \mathbf{V}(0)^* \mathbf{Z}^*) [\mathbf{L}^{-1}]^\dagger \\ \mathbf{V}(r) &= (\mathbf{V}(0) + \lambda \mathbf{U}(0)^* \mathbf{Z}^*) [\mathbf{L}^{-1}]^\dagger \end{aligned} \quad (15)$$

express the change in the quasiparticle amplitudes. By choosing various QTDA operators, we can obtain a set of basis states $|\Phi_r\rangle$ which are transformed using QTDA operators \hat{Z}_r . In the current work, we choose the 15 lowest-energy QTDA phonons, which is a computationally tractable choice. Since the QTDA evolution further breaks the conservation of particle numbers, we also compute the average proton number $\langle N_Z \rangle$ and neutron number $\langle N_N \rangle$ with the QTDA-transformed wavefunctions, to ensure the chosen QTDA-generated basis states gives the correct proton and neutron numbers approximately. Nonetheless, particle-number projection is required.

Once we have obtained a set of reference states, we project out states of good angular momenta as well as good proton and neutron numbers, $|JMK; NZ; r\rangle \equiv \hat{P}_{MK}^J \hat{P}^N \hat{P}^Z |\Phi_r\rangle$. Here \hat{P} 's projects onto well-defined angular momentum J and its z -component M , neutron number N , and proton number Z [8]. Using these states we construct the Hamiltonian kernel $\mathcal{H}_{MK}^J(r; s)$ and the norm kernel $\mathcal{N}_{MK}^J(r; s)$ are given by:

$$\begin{aligned} \mathcal{H}_{MK}^J(r; s) &= \langle \Phi_r | \hat{H} \hat{P}_{MK}^J \hat{P}^N \hat{P}^Z | \Phi_s \rangle, \\ \mathcal{N}_{MK}^J(r; s) &= \langle \Phi_r | \hat{P}_{MK}^J \hat{P}^N \hat{P}^Z | \Phi_s \rangle. \end{aligned} \quad (16)$$

We solve the generalized eigenvalue problem, which is really solving the discretized Hill-Wheeler equations [8]:

$$\sum_{K,s} \left\{ \mathcal{H}_{MK}^J(r; s) - E_\sigma^J \mathcal{N}_{MK}^J(r; s) \right\} f_{s\sigma}^{JK} = 0, \quad (17)$$

where σ labels the eigenstates. To solve Eq.(17), we diagonalize the norm kernel \mathcal{N} and use the nonzero eigenvalues and corresponding eigenvectors to construct a set of "natural states". Then, the Hamiltonian is diagonalized in the space of these natural states to obtain the GCM states $|\Psi_{NZ\sigma}^J\rangle$ (see details in Refs. [22, 23]). The GCM state is a superposition of projected states,

$$|\Psi_{NZ\sigma}^{J,M}\rangle = \sum_{K,s} f_{s\sigma}^{JK} |JMK; NZ; s\rangle, \quad (18)$$

using the weight functions $f_{s\sigma}^{JK}$, from Eq. (17).

We benchmark our QTDA-driven GCM by comparing results against those from full SM calculations, which can be considered numerically "exact" in a given model space, as well as a CHFB-GCM calculation, all using the same interaction Hamiltonian.

For this initial work we focus on the $0\nu\beta\beta$ decay candidate nuclei $^{124}\text{Sn}/\text{Te}$, $^{130}\text{Te}/\text{Xe}$, and $^{136}\text{Xe}/\text{Ba}$. These nuclei are expected to have near spherical or weak deformation. Unlike the well-deformed nuclei which are dominated by rotational behavior, one can expect that the vibrational motion and quasiparticle excitation, which can be described by QTDA, may compete with the rotational motion in the low-lying states of these nuclei. In addition, previous GCM calculations using axial deformation and pn pairing amplitudes as coordinates show about 30% overestimation of $0\nu\beta\beta$ matrix elements for these nuclei

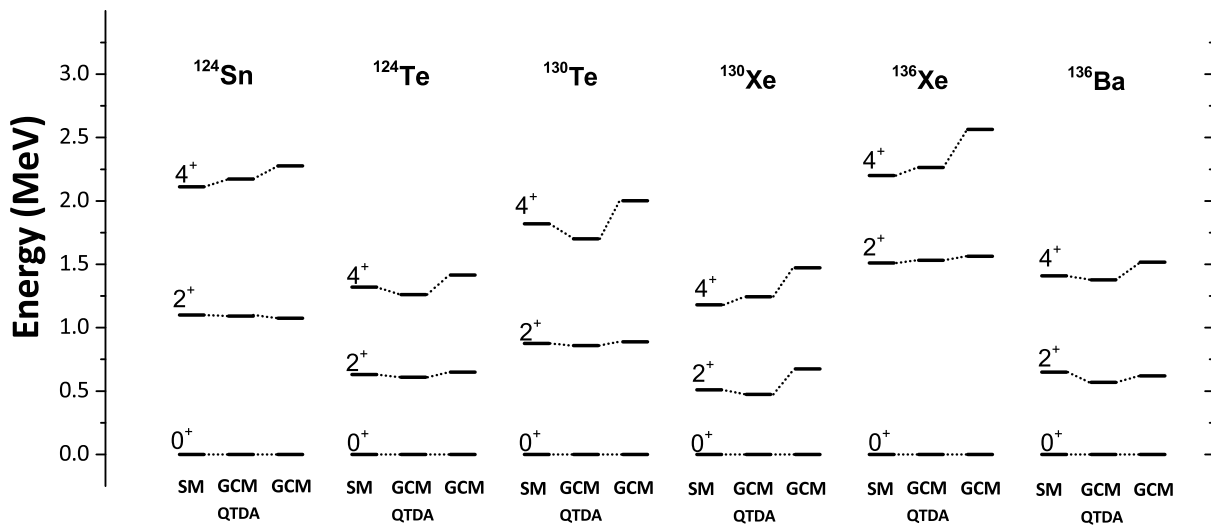


FIG. 1: The calculated low-lying energy levels for ^{124}Sn , ^{124}Te , ^{130}Te , ^{130}Xe , ^{136}Xe , and ^{136}Ba by using QTDA-driven GCM, compared to the constrained Hartree-Fock-Bogoliubov (CHFb) GCM [35] and the exact solutions of SM [44, 45].

when compared with the SM predictions, implying the lack of important correlations.

The shell-model effective Hamiltonian we use is called the singular value decomposition (SVD) Hamiltonian [46], which is fine tuned for the $jj55$ -shell configuration space that comprises the $0g_{7/2}$, $1d_{5/2}$, $1d_{3/2}$, $2s_{1/2}$, and $0h_{11/2}$ orbitals. This effective interaction has accounted successfully for the spectroscopy, electromagnetic transitions, and deformation of the initial and final nuclei that our calculations involve [44, 45].

Our CHFb-GCM calculation include axially-symmetric quadrupole deformation and pn pairing amplitude as the coordinates [35]. For ^{124}Te , ^{130}Te , ^{130}Xe , and ^{136}Ba , we generated 50 to 90 basis states, by constraining 9 to 12 different quadrupole moments and 6 to 8 different pn pairing amplitudes, respectively. The cases ^{124}Sn and ^{136}Xe lack valence protons and valence neutron holes, respectively, so one cannot change pn pairing; for those nuclides we use 13 basis states constrained to quadrupole moments only. It is important to note that as these nuclides have axially symmetric HFB minima, the standard calculations omit triaxially deformed configurations, so that angular momentum projection only evaluates integrals over the Euler angle β . (For other candidate $0\nu\beta\beta$ targets with naturally triaxial minima, e.g. ^{76}Ge , full three-dimensional projection unsurprisingly improves results [24].)

In our QTDA-driven GCM calculations we employ about 15 QTDA operators Z_r built on the HFB states. Aside from the base HFB minimum, we do not use any of the constrained reference states from the CHFb-GCM calculation. The nuclides ^{124}Te , ^{130}Te , ^{130}Xe , and ^{136}Ba have axially deformed HFB solutions, but since ^{124}Sn and ^{136}Xe have spherical minima, we constrain the base HFB states $|\Phi_0\rangle$ to axial quadrupole deformation $\beta_2 = 0$ and $\beta_2 = \pm 0.1$. While both the HFB state and the TDA

TABLE I: The g.s. energies (in MeV) obtained with SVD Hamiltonian by using CHFb-GCM, QTDA-driven GCM, and SM for ^{124}Sn , ^{124}Te , ^{130}Te , ^{130}Xe , ^{136}Xe , and ^{136}Ba .

Nuclei	CHFb-GCM	QTDA-GCM	SM
^{124}Sn	-15.733	-15.684	-16.052
^{124}Te	-23.082	-22.641	-24.446
^{130}Te	-25.705	-25.563	-26.039
^{130}Xe	-32.583	-32.220	-33.313
^{136}Xe	-34.931	-34.912	-34.971
^{136}Ba	-40.341	-40.176	-40.745

modes have good axial symmetry, that is, good J_z projection K , if a QTDA mode has $K \neq 0$, then exponentiated it mixes K . Thus we must project by quadrature over all three Euler angles. We also cannot use time-reversal and simplex symmetries which reduce by a factor of 16 the computational requirements of the quadrature [23]. Thus, although our current calculations have fewer reference states, the overall computational burden is significantly greater, requiring $\sim 2000\times$ more evaluations for a single matrix element. We emphasize this difference is largely because our CHFb-GCM code has been highly optimized for nuclides with axially symmetric minima. We have investigated efficient projection methods [47, 48] but have yet to implement them in projected HFB.

Figure 1 shows the low-lying level spectra of ^{124}Sn , ^{124}Te , ^{130}Te , ^{130}Xe , ^{136}Xe , and ^{136}Ba , compared to the CHFb-GCM calculation [35], as well as the SM calculations [44, 45]. Generally, the 2^+ states obtained from both CHFb-GCM and QTDA-driven GCM calculations are in reasonable agreement with the SM results and experimental spectra. CHFb-GCM calculations, however, tend to overestimate the excitation energies of 4^+ states. The overestimation could be due to the fact that the pre-

TABLE II: The $B(E2 : 0_1^+ \rightarrow 2_1^+)$ (in e^2b^2) obtained with SVD Hamiltonian by using CHFB-GCM [35], QTDA-driven GCM (this work), and SM [44, 45] for ^{124}Sn , ^{124}Te , ^{130}Te , ^{130}Xe , ^{136}Xe , and ^{136}Ba , compared to the adopted values [50].

	^{124}Sn	^{124}Te	^{130}Te	^{130}Xe	^{136}Xe	^{136}Ba
CHFB-GCM	0.168	0.648	0.165	0.492	0.220	0.475
QTDA-GCM	0.137	0.547	0.145	0.415	0.180	0.418
SM	0.146	0.579	0.153	0.502	0.215	0.479
Adopted	0.162	0.560	0.297	0.634	0.217	0.413

vious GCM calculations exclude the vibrational motion and broken-pair excitation, while these two excitation modes may lower the excited states significantly, especially in the nearly spherical and weakly deformed nuclei. Since the reference states generated by QTDA modes incorporate (at least partly) vibrational motion and two-quasiparticle excitations, our current results reduce the overestimation of 4^+ states. Inclusion of the vibrational motion and two-quasiparticle configurations is, indeed, important for a better description of the low-lying spectra of spherical and weakly deformed nuclei.

Conversely, the ground state energies, shown in Table I, are about 50 to 350 keV higher for our current QTDA-driven GCM than for the CHFB-GCM, which in turn is about 40 keV to 1.4 MeV above the numerically exact SM energies, a failing for GCM calculations previously known [49]. Keep in mind that our QTDA-driven GCM has fewer reference states than CHFB-GCM.

For the calculation of the reduced E2 transition probability $B(E2 : 0_1^+ \rightarrow 2_1^+)$, we use the canonical effective charges $e_n^{\text{eff}} = 0.5e$ and $e_p^{\text{eff}} = 1.5e$ for $^{130}\text{Te}/\text{Xe}$ and $^{136}\text{Xe}/\text{Ba}$. For $^{124}\text{Sn}/\text{Te}$, we use $e_n^{\text{eff}} = 0.88e$ and $e_p^{\text{eff}} = 1.88e$, which are suggested for tin isotopes with no protons in the valence space in Refs. [45, 46]. The results are compared in Table II against SM results [44, 45], and CHFB-GCM [35], as well as the experimentally adopted values [50]. We see a good agreement amongst our QTDA-driven GCM, CHFB-GCM, and SM calculations. Both GCM and SM calculations reproduce well the adopted values with only a slight underestimation for ^{130}Te and ^{130}Xe . While the underestimation, also mentioned in Ref. [44], suggests the effective charges should be adjusted, for our purposes we are interested in comparison of the calculations.

As an application of our QTDA-driven GCM, we compute the values of $0\nu\beta\beta$ decay matrix elements of ^{124}Sn , ^{130}Te , and ^{136}Xe . The results are listed in Table III, where we show the Gamow-Teller, the Fermi, and the tensor contributions respectively. The total matrix elements given by QTDA-driven GCM are smaller than those of CHFB-GCM, in closer agreement with exact SM diagonalization.

In the closure approximation, one computes the $0\nu\beta\beta$ matrix element of a two-body transition operator between the initial and final ground states. Assuming an

TABLE III: The nuclear matrix elements obtained with SVD Hamiltonian by using CHFB-GCM[35], QTDA-driven GCM (this work), and SM [44, 45] for ^{124}Sn , ^{130}Te , and ^{136}Xe . CD-Bonn SRC parametrization was used.

		$M_{\text{GT}}^{0\nu}$	$M_{\text{F}}^{0\nu}$	$M_{\text{T}}^{0\nu}$	$M^{0\nu}$
^{124}Sn	CHFB-GCM	2.48	-0.51	-0.03	2.76
	QTDA-GCM	2.08	-0.73	-0.01	2.53
	SM	1.85	-0.47	-0.01	2.15
^{130}Te	CHFB-GCM	2.25	-0.47	-0.02	2.52
	QTDA-GCM	1.97	-0.69	-0.01	2.39
	SM	1.66	-0.44	-0.01	1.94
^{136}Xe	CHFB-GCM	2.17	-0.32	-0.02	2.35
	QTDA-GCM	1.65	-0.50	-0.01	1.96
	SM	1.50	-0.40	-0.01	1.76

exchange of a light Majorana neutrino with the usual left-handed currents, the matrix element is [31]:

$$M^{0\nu} = M_{\text{GT}}^{0\nu} - \frac{g_V^2}{g_A} M_{\text{F}}^{0\nu} + M_{\text{T}}^{0\nu} \quad (19)$$

where GT, F, and T refer to the Gamow-Teller, Fermi and tensor parts of the matrix elements. The vector and axial coupling constants are taken to be $g_V = 1$ and $g_A = 1.254$, respectively. The wave functions are modified at short distances using a Jastrow short-range correlation (SRC) function with CD-Bonn parametrization [31, 51].

The CHFB-GCM agrees well with the SM for the Fermi contribution, but overestimates the Gamow-Teller contribution by about 30% [35]. By contrast, QTDA-driven GCM improves considerably the agreement of the Gamow-Teller contribution, although both Gamow-Teller and Fermi are still slightly overestimated. This suggests correlations beyond quadrupole and pn -pairing are important.

In this paper, we present a new Hamiltonian-based GCM calculation. In this approach, we include low-lying vibrational modes, derived from QTDA, to evolve the HFB minimum via Thouless' theorem to generate reference states. These reference states are then projected to have good particle number and angular momentum. To show the reliability of the new QTDA-driven GCM calculation, we apply it to weakly deformed nuclides and $0\nu\beta\beta$ decay candidate nuclei pairs $^{124}\text{Sn}/\text{Te}$, $^{130}\text{Te}/\text{Xe}$, and $^{136}\text{Xe}/\text{Ba}$, and compared the low-lying level spectra, the reduced $E2$ transition probabilities $B(E2 : 0_1^+ \rightarrow 2_1^+)$, and the $0\nu\beta\beta$ decay matrix elements, against exact diagonalization SM results, as well as CHFB-GCM calculations based on the HFB states constrained to different amount of collectivity (i.e., deformation, isovector pairing, isoscalar pairing, *etc.*), all using the same interaction Hamiltonian. Our QTDA-driven GCM results are in reasonable agreement with the SM, competitive with and in some cases outperforming CHFB-GCM calculations.

In the near future we will investigate the efficiency of QTDA-driven GCM; for example, K -mixing by TDA modes requires more burdensome computation, and it is

worth to see if it is practical to constrain it. In addition, we see two avenues for further improvements. The first is to add more reference states. Furthermore, one could evolve HFB states constrained to quadrupole deformation, isoscalar pairing correlation, *etc.*, or simply combine the reference states of CHFB- and QTDA-driven GCM; the results of Tables I and II suggests this may be a useful or even necessary strategy. The other option is, instead of QTDA, one could try quasiparticle random phase approximation (QRPA) operators, which would incorporate two-particle two-hole components into the ground state. While more complicated, this could improve the descrip-

tion of the ground state, and hence a better description $0\nu\beta\beta$ decay nuclear matrix elements needed to interpret experiments.

This material is based upon work supported by the U.S. Department of Energy, Office of Science, Office of Nuclear Physics, under Award Number DE-FG02-03ER41272, and by U.S. Department of Energy Topical Collaboration Grant No. DE-SC0015376, and of the National Energy Research Scientific Computing Center, a DOE Office of Science User Facility supported by the Office of Science of the U.S. Department of Energy under Contract No. DE-AC02-05CH11231

-
- [1] F. T. Avignone, S. R. Elliott, and J. Engel, *Rev. Mod. Phys.* **80**, 481 (2008).
- [2] J. Menéndez, *Journal of Physics G: Nuclear and Particle Physics* **45**, 014003 (2017).
- [3] J. Engel and J. Menéndez, *Rep. Prog. Phys.* **80**, 046301 (2017).
- [4] J. Engel, S. Pittel, and P. Vogel, *International Journal of Modern Physics E* **1**, 1 (1992).
- [5] R. J. Gaitskell, *Annu. Rev. Nucl. Part. Sci.* **54**, 315 (2004).
- [6] N. Anand, A. L. Fitzpatrick, and W. C. Haxton, *Phys. Rev. C* **89**, 065501 (2014).
- [7] P. Brussard and P. Glaudemans, *Shell-model applications in nuclear spectroscopy* (North-Holland Publishing Company, Amsterdam, 1977).
- [8] P. Ring and P. Schuck, *The Nuclear Many-Body Problem* (Springer-Verlag, Berlin, 1980).
- [9] S. C. Pieper, *Nuclear Physics A* **751**, 516 (2005).
- [10] G. Hagen, T. Papenbrock, D. J. Dean, and M. Hjorth-Jensen, *Physical Review C* **82**, 034330 (2010).
- [11] H. Hergert, S. Bogner, T. Morris, A. Schwenk, and K. Tsukiyama, *Physics Reports* **621**, 165 (2016).
- [12] B. A. Brown and B. H. Wildenthal, *Annual Review of Nuclear and Particle Science* **38**, 29 (1988).
- [13] E. Caurier, G. Martínez-Pinedo, F. Nowacki, A. Poves, and A. P. Zuker, *Reviews of Modern Physics* **77**, 427 (2005).
- [14] P. Navrátil, J. Vary, and B. Barrett, *Physical Review C* **62**, 054311 (2000).
- [15] B. R. Barrett, P. Navrátil, and J. P. Vary, *Progress in Particle and Nuclear Physics* **69**, 131 (2013).
- [16] M. Bender, P.-H. Heenen, and P.-G. Reinhard, *Rev. Mod. Phys.* **75**, 121 (2003).
- [17] M. Honma, T. Mizusaki, and T. Otsuka, *Phys. Rev. Lett.* **77**, 3315 (1996).
- [18] T. Otsuka, M. Honma, T. Mizusaki, N. Shimizu, and Y. Utsuno, *Progress in Particle and Nuclear Physics* **47**, 319 (2001).
- [19] R. Rodríguez-Guzmán, J. L. Egidio, and L. M. Robledo, *Phys. Rev. C* **65**, 024304 (2002).
- [20] T. Nikšić, D. Vretenar, and P. Ring, *Phys. Rev. C* **74**, 064309 (2006).
- [21] M. Bender and P.-H. Heenen, *Phys. Rev. C* **78**, 024309 (2008).
- [22] J. M. Yao, J. Meng, P. Ring, and D. Vretenar, *Phys. Rev. C* **81**, 044311 (2010).
- [23] T. R. Rodríguez and J. L. Egidio, *Phys. Rev. C* **81**, 064323 (2010).
- [24] C. F. Jiao, J. Engel, and J. D. Holt, *Phys. Rev. C* **96**, 054310 (2017).
- [25] P. Bonche, S. J. Krieger, M. S. Weiss, J. Dobaczewski, H. Flocard, and P.-H. Heenen, *Phys. Rev. Lett.* **66**, 876 (1991).
- [26] J. M. Yao, E. F. Zhou, and Z. P. Li, *Phys. Rev. C* **92**, 041304 (2015).
- [27] P.-H. Heenen, A. Valor, M. Bender, P. Bonche, and H. Flocard, *Eur. Phys. J. A* **11**, 393 (2001).
- [28] N. L. Vaquero, T. R. Rodríguez, and J. L. Egidio, *Phys. Rev. Lett.* **111**, 142501 (2013).
- [29] P. Vogel and M. R. Zirnbauer, *Phys. Rev. Lett.* **57**, 3148 (1986).
- [30] J. Engel, P. Vogel, and M. R. Zirnbauer, *Phys. Rev. C* **37**, 731 (1988).
- [31] F. Šimković, A. Faessler, V. Rodin, P. Vogel, and J. Engel, *Phys. Rev. C* **77**, 045503 (2008).
- [32] M. T. Mustonen and J. Engel, *Phys. Rev. C* **87**, 064302 (2013).
- [33] N. Hinohara and J. Engel, *Phys. Rev. C* **90**, 031301(R) (2014).
- [34] J. Menéndez, N. Hinohara, J. Engel, G. Martínez-Pinedo, and T. R. Rodríguez, *Phys. Rev. C* **93**, 014305 (2016).
- [35] C. F. Jiao, M. Horoi, and A. Neacsu, *Phys. Rev. C* **98**, 064324 (2018).
- [36] B. Jancovici and D. Schiff, *Nuclear Physics* **58**, 678 (1964).
- [37] G. H. Lang, C. W. Johnson, S. E. Koonin, and W. E. Ormand, *Phys. Rev. C* **48**, 1518 (1993).
- [38] S. E. Koonin, D. J. Dean, and K. Langanke, *Physics reports* **278**, 1 (1997).
- [39] G. Puddu, P. F. Bortignon, and R. A. Broglia, *Phys. Rev. C* **42**, R1830 (1990).
- [40] Z.-C. Gao and M. Horoi, *Phys. Rev. C* **79**, 014311 (2009).
- [41] F.-Q. Chen and J. L. Egidio, *Phys. Rev. C* **95**, 024307 (2017).
- [42] J. Suhonen, *From nucleons to nucleus: concepts of microscopic nuclear theory* (Springer Science & Business Media, 2007).
- [43] J. Egidio, J. Lessing, V. Martin, and L. Robledo, *Nuclear Physics A* **594**, 70 (1995).
- [44] A. Neacsu and M. Horoi, *Phys. Rev. C* **91**, 024309 (2015).

- [45] M. Horoi and A. Neacsu, *Phys. Rev. C* **93**, 024308 (2016).
- [46] C. Qi and Z. X. Xu, *Phys. Rev. C* **86**, 044323 (2012).
- [47] C. W. Johnson and K. D. O'Mara, *Phys. Rev. C* **96**, 064304 (2017).
- [48] C. W. Johnson and C. Jiao, *Journal of Physics G: Nuclear and Particle Physics* **46**, 015101 (2018).
- [49] J. M. Yao, J. Engel, L. J. Wang, C. F. Jiao, and H. Hergert, *Phys. Rev. C* **98**, 054311 (2018).
- [50] B. Pritychenko, M. Birch, B. Singh, and M. Horoi, *Atomic Data and Nuclear Data Tables* **107**, 1 (2016).
- [51] F. Šimkovic, A. Faessler, H. Mütter, V. Rodin, and M. Stauf, *Phys. Rev. C* **79**, 055501 (2009).